Electronic supporting information

Nickel silicate MFI-type zeolite catalyst prepared by interzeolite transformation: Tailoring the catalytic active sites for glucose conversion†

Sungjoon Kweon,[a] Yunhye Cho,[a] Jun Seong Park,[a] Jiae Ryu,[b] Chang Geun Yoo,[b] Hyung-Ki Min[c] and Min Bum Park*[ab]

[a]*Department of Energy and Chemical Engineering, Incheon National University, Incheon 22012, Korea*

[b]*Department of Chemical Engineering, State University of New York College of Environmental Science and Forestry, Syracuse, New York 13210, United States*

[c]*Hydrogen & C1 Gas Research Center, Korea Research Institute of Chemical Technology, Daejeon 34114, Korea*

†Electronic supplementary information (ESI) available. See DOI: xxx

Table S1 Relative ratios of intermediate Ni and isolated Ni of Ni-MFI(x)(y) solids determined by UV-DRS, Ni 2p XPS, and CD_3CN-IR

Sample[a]	Crystallization time (h)	$Ni_{intermediate}/Ni_{isolated}$		
		UV-DRS[b]	Ni 2p XPS[c]	CD_3CN-IR[d]
Ni-MFI(135)	1	1.29	1.22	1.27
	3	1.65	1.70	1.67
	6	1.82	1.85	1.83
	12	1.88	1.89	1.93
	24	1.70	1.70	1.68
	72	1.73	1.76	1.80
	168	1.29	1.27	1.25
Ni-MFI(150)	1	1.45	1.41	1.43
	3	1.54	1.56	1.50
	6	1.30	1.42	1.29
	12	1.39	1.39	1.33
	24	0.64	0.65	0.62
	72	0.57	0.58	0.56
	168	0.43	0.47	0.43
Ni-MFI(190)	1	1.50	1.51	1.50
	3	0.74	0.76	0.74
	6	0.50	0.51	0.50
	12	0.17	0.16	0.17
	24	0.13	0.13	0.15
	72	0.12	0.10	0.12
	168	0.10	0.08	0.10

[a] Calcined at 550 °C for 8 h. [b] Determined by the relative ratio of integrated areas of UV absorption peaks at around 260 and 200 nm. [c] Determined by the relative ratio of the integrated areas of Ni $2p_{3/2}$ XPS peaks at around 757.5 and 758.1 eV. [d] Determined by the relative ratio of the integrated areas of CD_3CN-absorption IR peaks at around 2306 and 2311 cm^{-1}.

Table S2 Binding energies of Ni $2p_{3/2}$ and Si 2p XPS spectra for Ni-MFI(x)(y) solids prepared in this study

Sample[a]	Crystallization time (h)	Binding energy (eV)				
		Ni $2p_{3/2}$		Si 2p	$\Delta E_{\text{Ni-Si}}$[b]	
Ni-MFI(135)	1	857.5	858.1	104.3	753.2	753.8
	3	857.5	858.1	104.2	753.3	753.9
	6	857.5	858.4	104.5	753.0	753.9
	12	857.7	858.1	104.6	753.1	753.5
	24	857.8	858.2	104.6	753.2	753.6
	72	857.5	858.1	104.1	753.4	754.0
	168	857.5	858.0	104.2	753.3	753.8
Ni-MFI(150)	1	857.6	858.0	104.5	753.1	753.5
	3	857.5	858.2	104.4	753.1	753.8
	6	857.6	858.1	104.5	753.1	753.6
	12	857.7	858.5	104.6	753.1	753.9
	24	857.5	858.1	104.3	753.2	753.8
	72	857.3	858.0	104.3	753.0	753.7
	168	857.7	858.3	104.5	753.2	753.8
Ni-MFI(190)	1	857.2	858.2	104.2	753.0	754.0
	3	857.5	858.1	104.4	753.1	753.7
	6	857.6	858.1	104.3	753.3	753.8
	12	857.5	858.0	104.1	753.4	753.9
	24	857.2	858.0	104.1	753.1	753.9
	72	857.3	858.0	104.1	753.2	753.9
	168	857.2	858.0	104.2	753.0	753.8

[a] Calcined at 550 °C for 8 h. [b] Binding energy differences between Ni $2p_{3/2}$ and Si 2p XPS peaks.

Table S3 Amounts of water adsorbed on Ni-MFI(x)(y) solids prepared in this study

Sample[a]	Crystallization time (h)	Water (wt. %)[b]
Ni-MFI(135)	1	5.9
	3	7.7
	6	6.0
	12	6.2
	24	5.5
	72	4.5
	168	4.2
Ni-MFI(150)	1	4.7
	3	4.8
	6	4.2
	12	3.2
	24	3.1
	72	2.8
	168	2.7
Ni-MFI(190)	1	3.1
	3	2.8
	6	2.8
	12	2.3
	24	1.8
	72	1.7
	168	1.3

[a] Calcined at 550 °C for 8 h. [b] Determined by the weight loss at RT–100 °C in TGA/DTA of calcined Ni-MFI(x)(y) solids exposed for 1 d in ambient condition (Fig. S20†).

Table S4 Acidities of Ni-MFI(x)(y) solids determined by IR spectra after pyridine adsorption at 100–450 °C

Sample[a]	Crystallization time (h)	Concentration of Lewis / Brønsted acid sites (μmol g^{-1})[b]					Reduction rate (%)[c]	
		100 °C	200 °C	300 °C	400 °C	450 °C	Lewis	Brønsted
Ni-MFI(135)	1	434 / 64	125 / 43	14 / 19	– / –	– / –	97	71
	3	355 / 79	111 / 47	6 / 24	– / –	– / –	98	69
	6	326 / 85	54 / 53	1 / 28	– / –	– / –	100	67
	12	282 / 93	38 / 47	1 / 20	– / –	– / –	100	78
	24	226 / 83	34 / 71	1 / 31	– / –	– / –	100	63
	72	268 / 76	28 / 46	7 / 20	– / –	– / –	98	75
	168	174 / 89	34 / 68	1 / 35	– / –	– / –	99	61
Ni-MFI(150)	1	221 / 74	58 / 52	45 / 41	– / –	– / –	95	44
	3	204 / 85	28 / 65	14 / 39	– / –	– / –	93	55
	6	213 / 80	29 / 58	3 / 43	– / –	– / –	98	46
	12	216 / 98	28 / 82	9 / 56	– / –	– / –	96	42
	24	238 / 72	34 / 37	24 / 31	– / –	– / –	90	57
	72	241 / 70	40 / 43	37 / 37	– / –	– / –	85	48
	168	253 / 68	50 / 41	40 / 34	– / –	– / –	84	50
Ni-MFI(190)	1	210 / 77	46 / 57	29 / 34	– / 15	– / –	89	43
	3	198 / 58	26 / 55	25 / 28	– / 16	– / –	87	52
	6	250 / 47	65 / 35	35 / 25	– / 11	– / –	86	48
	12	259 / 36	47 / 32	36 / 19	– / 10	– / –	86	46
	24	288 / 25	65 / 12	46 / 11	– / –	– / –	84	54
	72	294 / 28	81 / 23	53 / 15	– / –	– / –	82	46
	168	322 / 28	66 / 19	62 / 15	– / –	– / –	81	46

[a] Calcined at 550 °C for 8 h. [b] The concentrations of Lewis and Brønsted acid sites were determined from the intensities of the py-IR bands at approximately 1450 and 1550 cm^{-1}, respectively (Figs. S21–S23†). [c] Reduction rate of Brønsted and Lewis acid concentrations determined between 100 and 300 °C.

Table S5 Comparison of catalytic results for glucose conversion between this work and previous studies

Catalyst	Glucose conversion condition			Glucose conversion (%)	5-HMF yield (%)	Ref.
	Temp. (°C)	Time (h)	Solvent			
Ni-MFI(190)(1)	160	24	DMSO + DI water	81	40	This study
$LaCl_3$ + HCl	170	4	NaCl + DI water	87	38	16
Sn-Beta + HCl	160	1.5	1-Butanol + DI water	77	20	23
H_3PO_4–carbon–$FePO_4$(0.15)	160	1.5	Acetone + DI water	58	22	59
Ta_2O_5	175	1.5	MIBK + DI water	69	23	60
Al-MCM-41	195	2.5	MIBK + DI water	87	36	61
0.2-SnOx/C-500	170	2	THF + DI water	77	35	62
U66SA	150	24	DMSO + DI water	23	35	63
TaPO	170	1	MIBK + DI water	56	33	64
MIL-101(Cr, Sn)-0.1	140	1	NaCl + DMAc	75	33	65

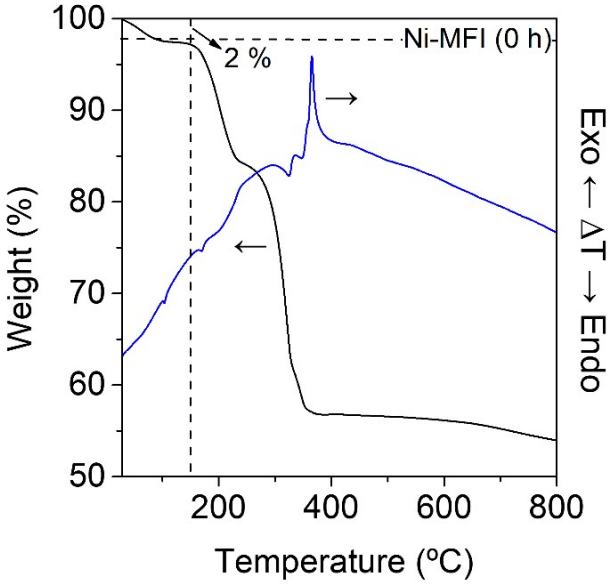

Fig. S1 TGA/DTA curves of dried powder denoted as Ni-MFI(0 h).

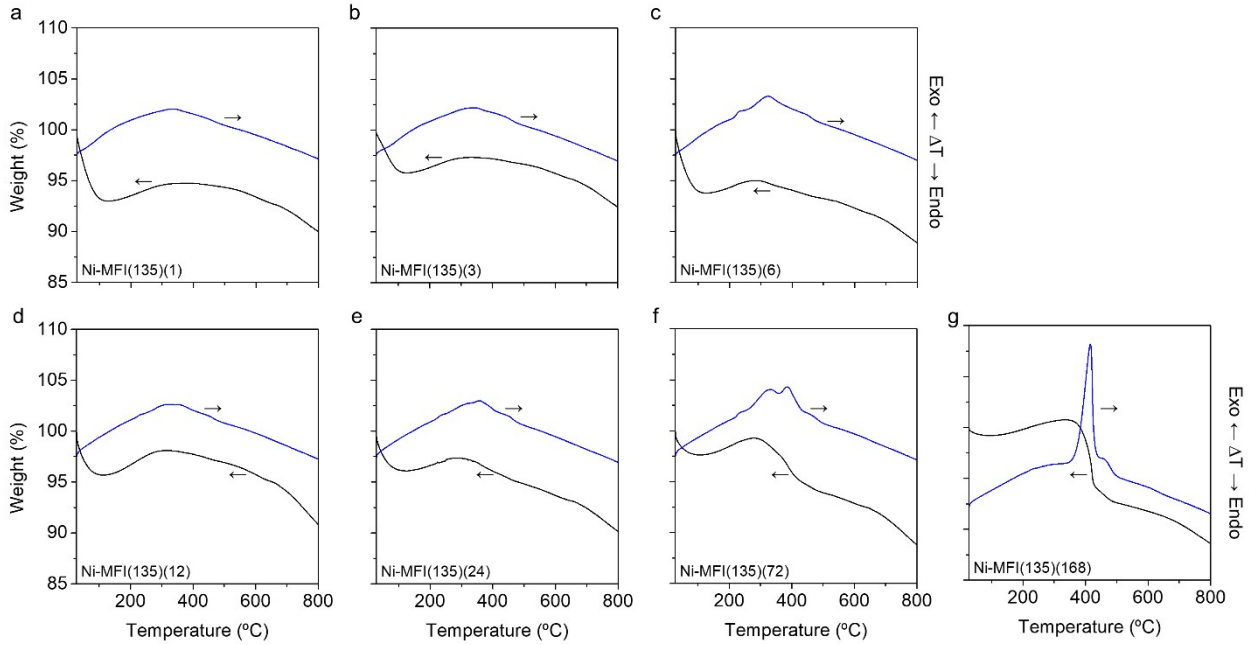

Fig. S2 TGA/DTA curves of Ni-MFI(x)(y) solids synthesized at 135 °C for (a) 1 h, (b) 3 h, (c) 6 h, (d) 12 h, (e) 24 h, (f) 72 h, and (g) 168 h.

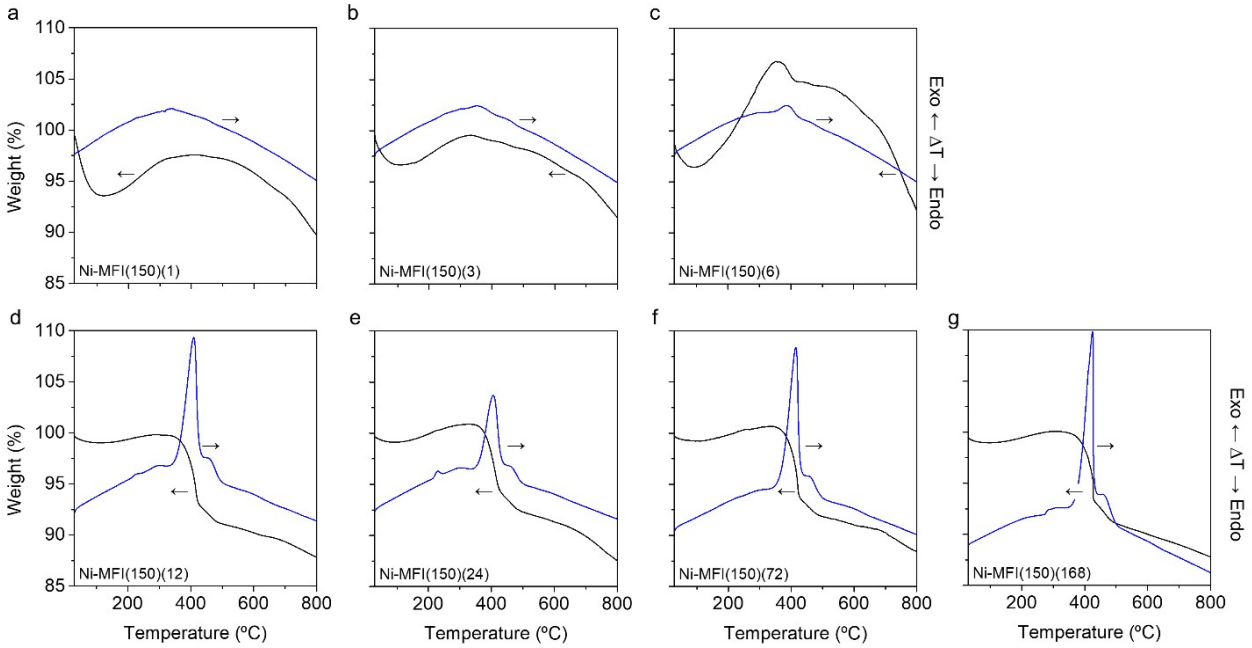

Fig. S3 TGA/DTA curves of Ni-MFI(*x*)(*y*) solids synthesized at 150 °C for (a) 1 h, (b) 3 h, (c) 6 h, (d) 12 h, (e) 24 h, (f) 72 h, and (g) 168 h.

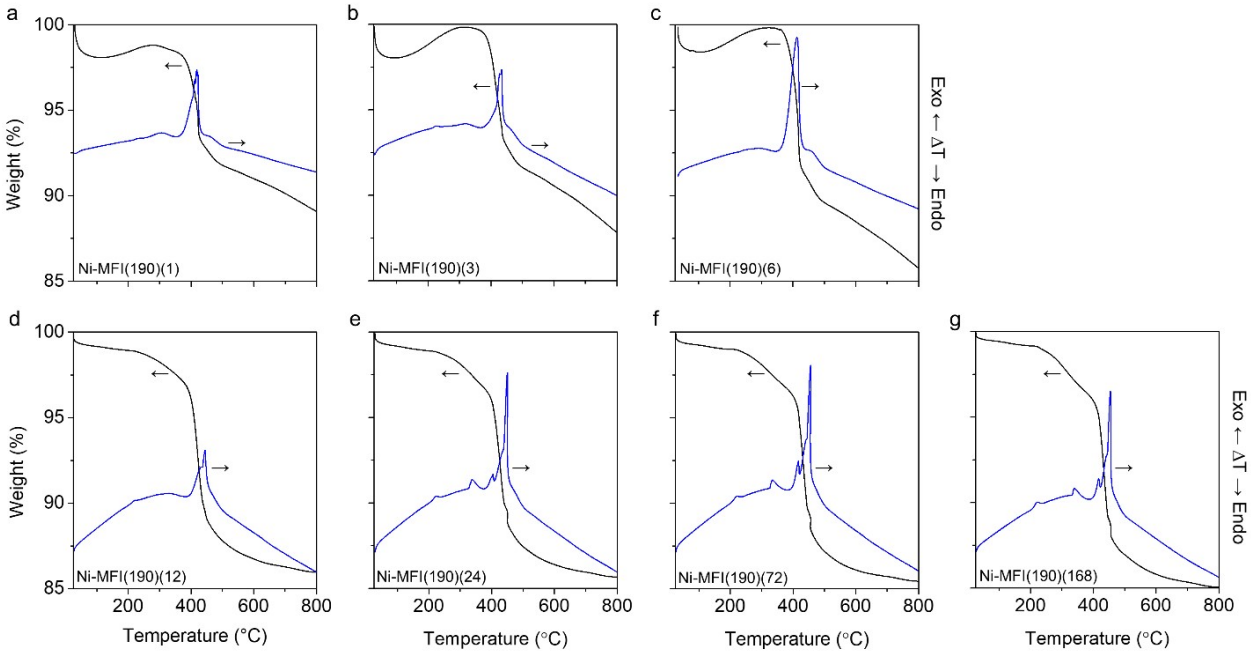

Fig. S4 TGA/DTA curves of Ni-MFI(x)(y) solids synthesized at 190 °C for (a) 1 h, (b) 3 h, (c) 6 h, (d) 12 h, (e) 24 h, (f) 72 h, and (g) 168 h.

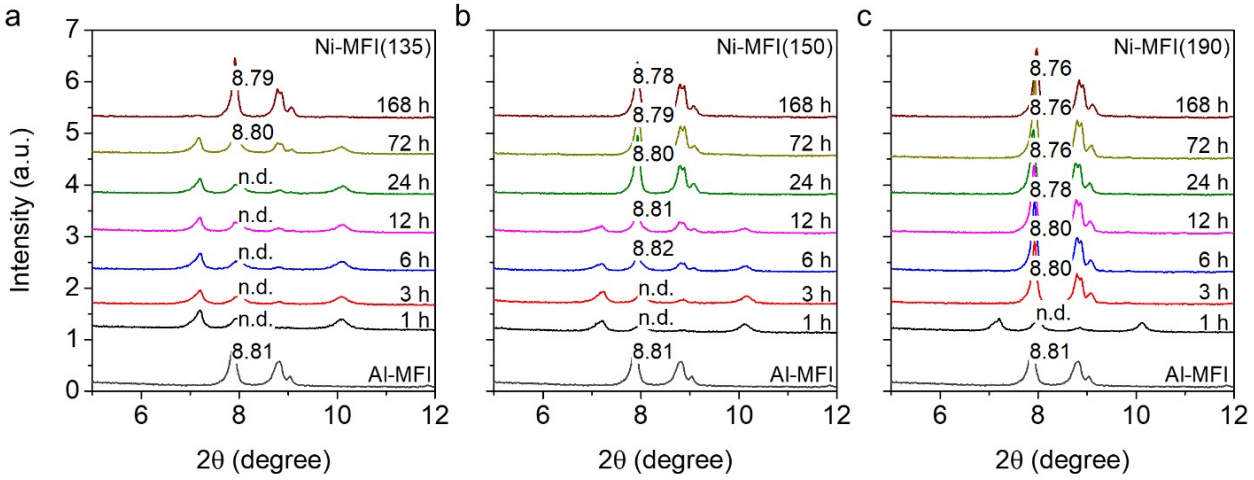

Fig. S5 Powder XRD patterns of Ni-MFI(x)(y) solids synthesized at (a) 135 °C, (b) 150 °C, and (c) 190 °C in the magnified 2θ = 5–12°. For comparison, the pattern of Al-MFI was added.

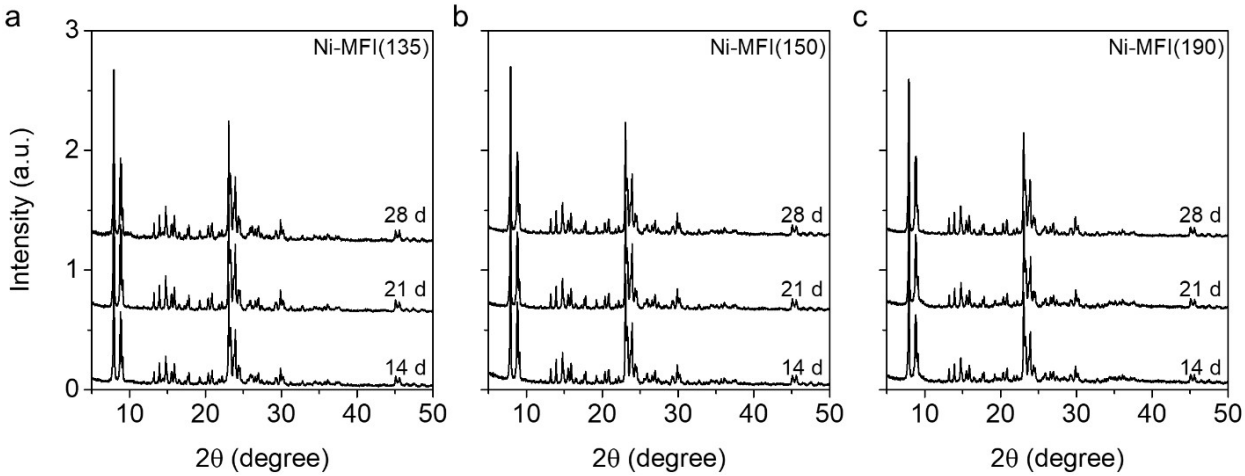

Fig. S6 Powder XRD patterns of Ni-MFI(*x*)(*y*) solids synthesized at (a) 135 °C, (b) 150 °C, and (c) 190 °C for 14–28 d.

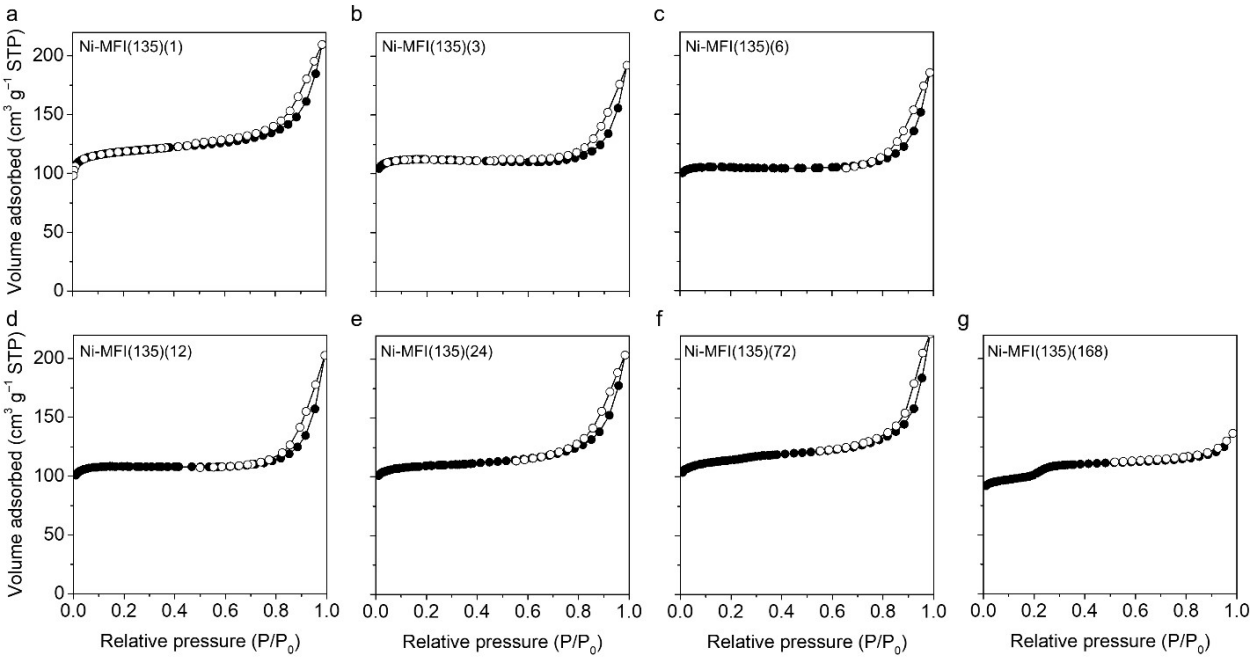

Fig. S7 N_2 sorption isotherms of Ni-MFI(*x*)(*y*) solids synthesized at 135 °C for (a) 1 h, (b) 3 h, (c) 6 h, (d) 12 h, (e) 24 h, (f) 72 h, and (g) 168 h.

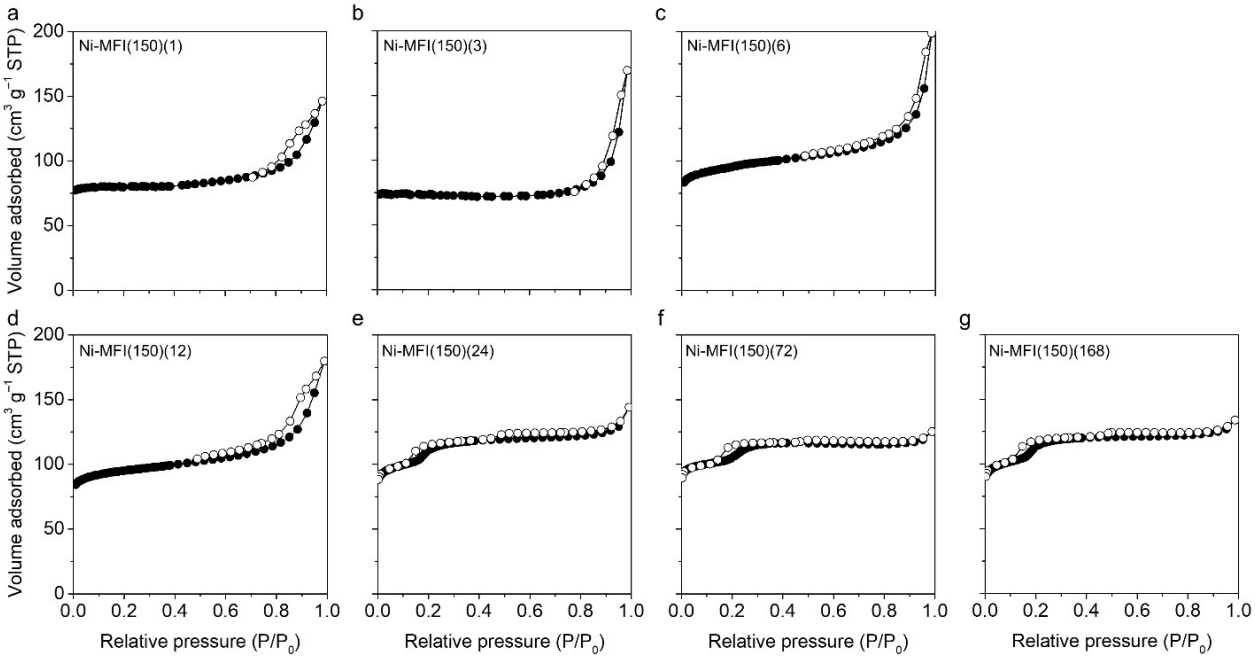

Fig. S8 N_2 sorption isotherms of Ni-MFI(x)(y) solids synthesized at 150 °C for (a) 1 h, (b) 3 h, (c) 6 h, (d) 12 h, (e) 24 h, (f) 72 h, and (g) 168 h.

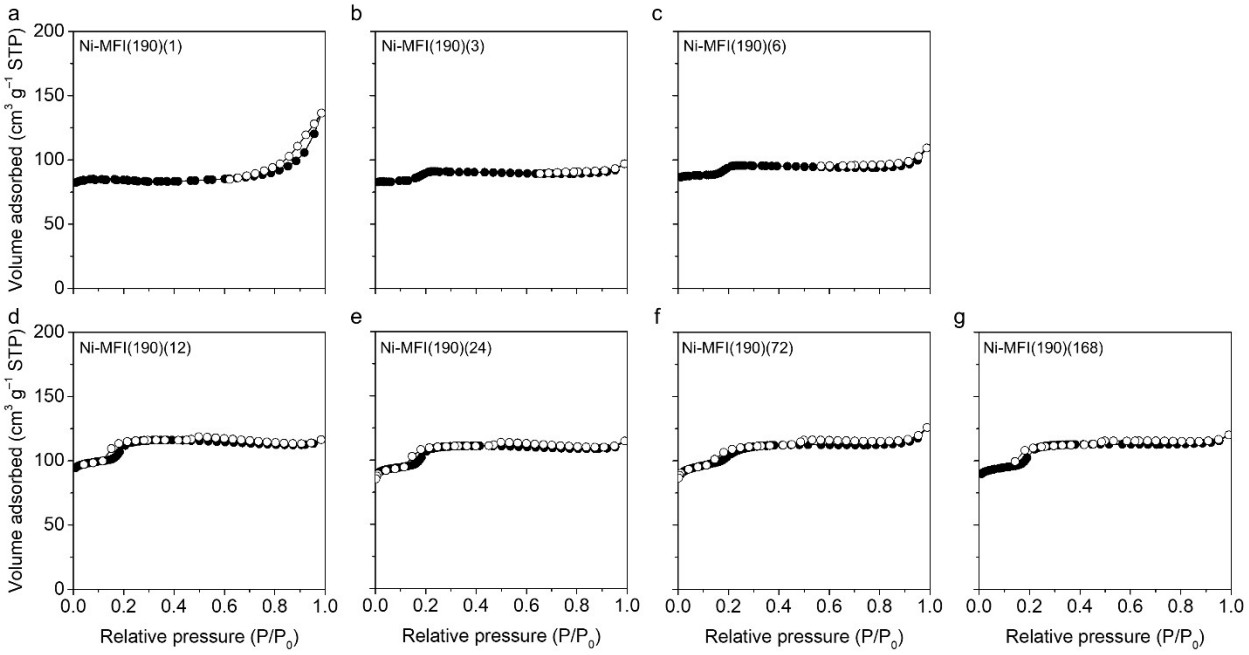

Fig. S9 N_2 sorption isotherms of Ni-MFI(*x*)(*y*) solids synthesized at 190 °C for (a) 1 h, (b) 3 h, (c) 6 h, (d) 12 h, (e) 24 h, (f) 72 h, and (g) 168 h.

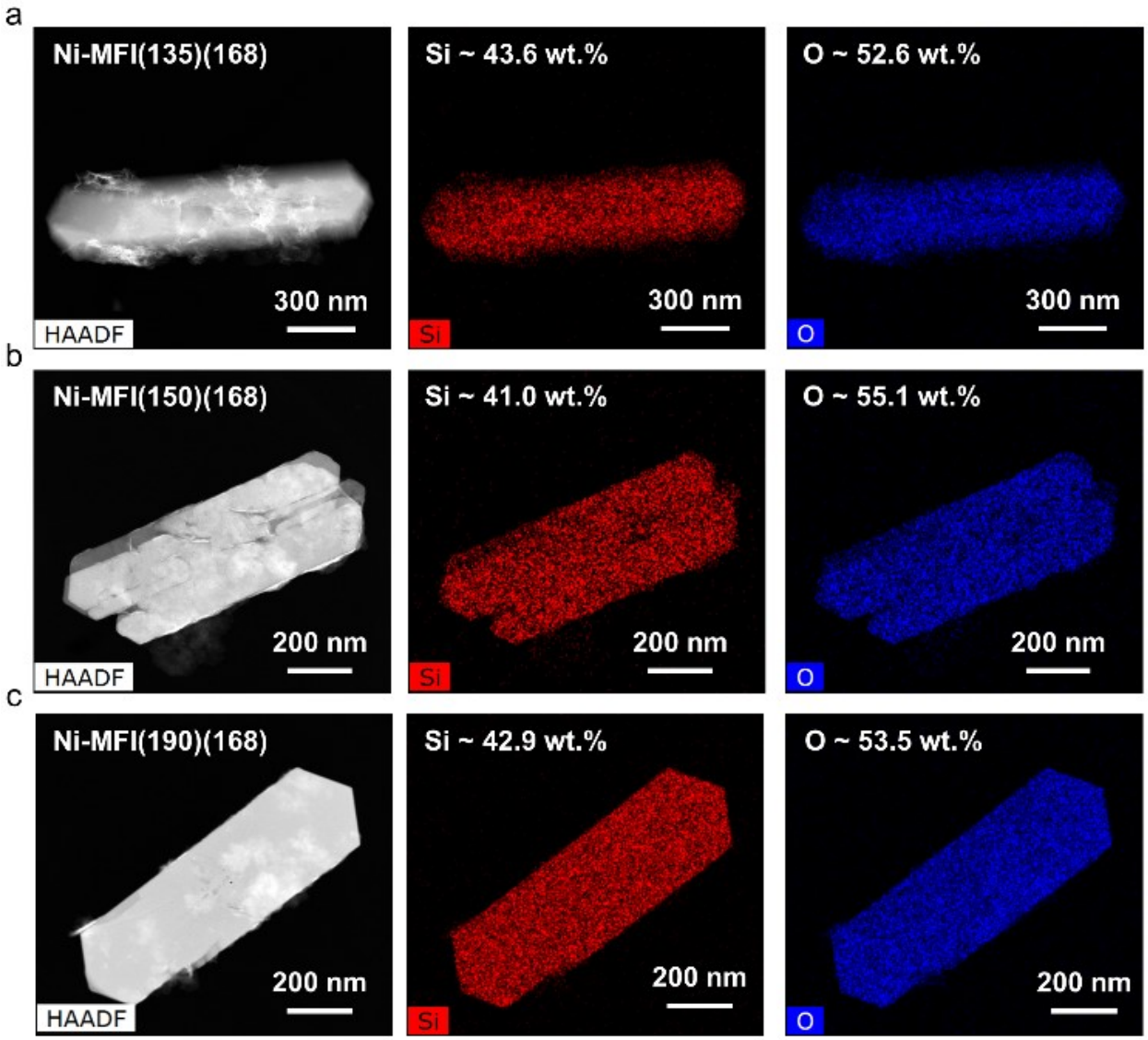

Fig. S10 STEM-EDS images of (a) Ni-MFI(135)(168), (b) Ni-MFI(150)(168), and (c) Ni-MFI(190)(168).

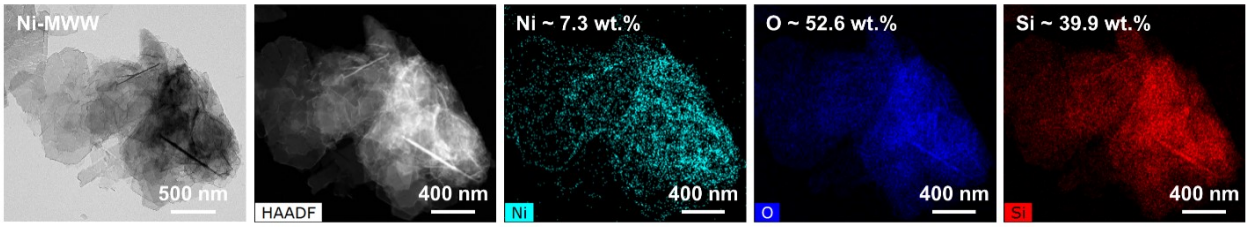

Fig. S11 (S)TEM-EDS images of Ni-MWW.

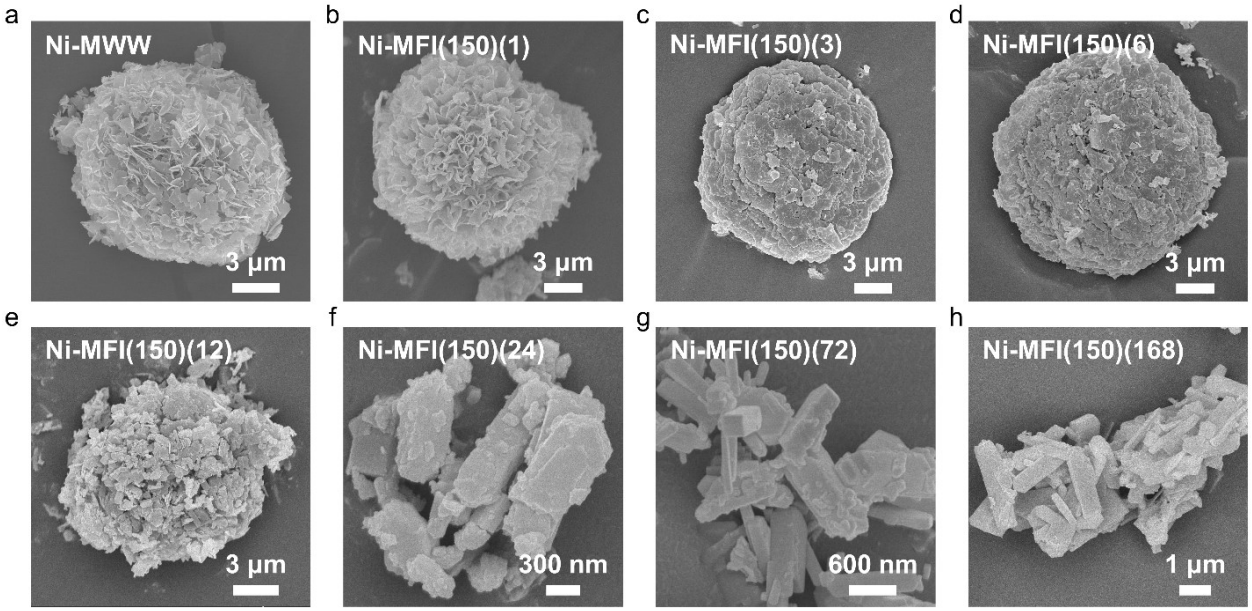

Fig. S12 SEM images of (a) Ni-MWW and Ni-MFI(x)(y) solids synthesized at 150 °C for (b) 1 h, (c) 3 h, (d) 6 h, (e) 12 h, (f) 24 h, (g) 72 h, and (h) 168 h.

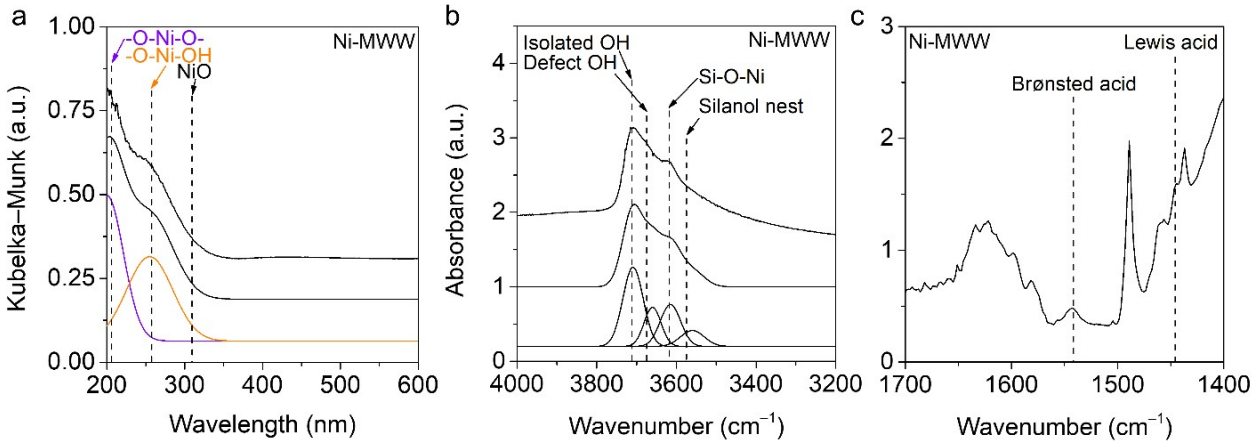

Fig. S13 (a) UV-DRS and (b) OH-IR spectra: experimental (top), simulated (middle), and deconvoluted components (bottom), and (c) py-IR spectra after pyridine adsorption at 100 °C of Ni-MWW.

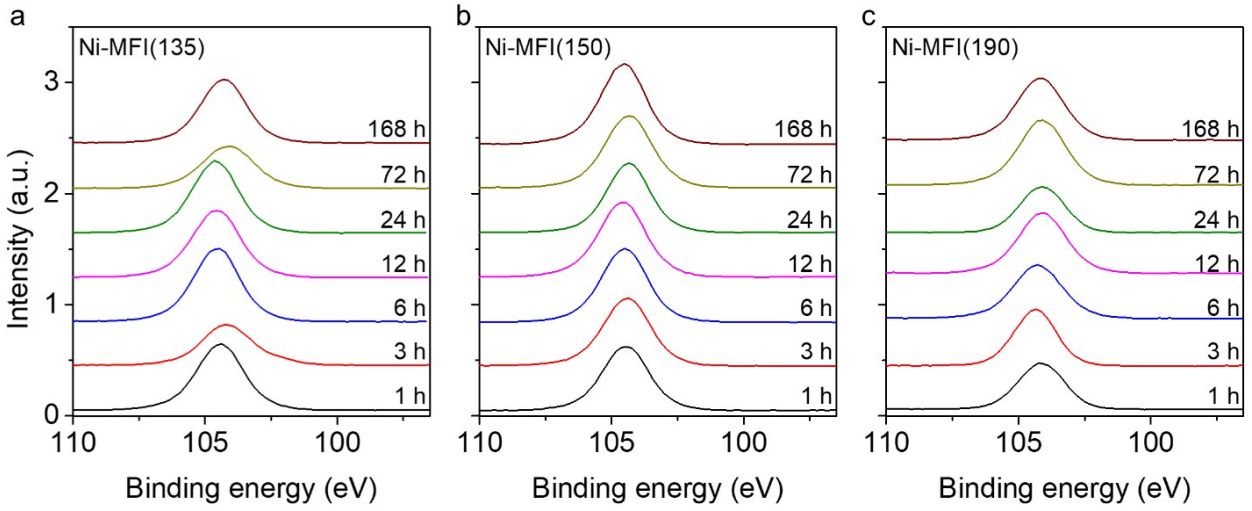

Fig. S14 Si 2p XPS spectra of Ni-MFI(x)(y) solids synthesized at (a) 135 °C, (b) 150 °C, and (c) 190 °C for the different crystallization times (1–168 h).

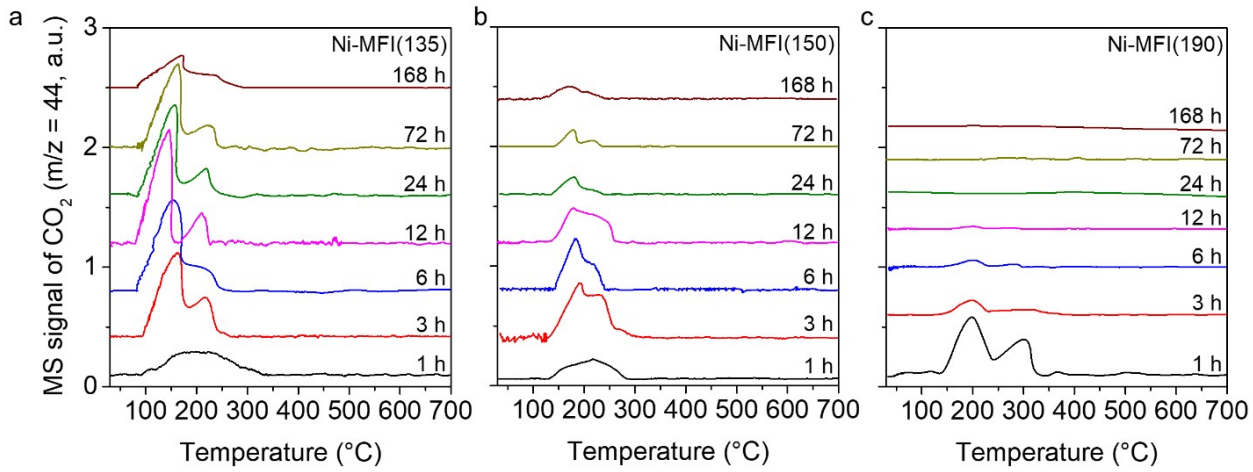

Fig. S15 CO_2 TPD profiles of Ni-MFI(x)(y) solids synthesized at (a) 135 °C, (b) 150 °C, and (c) 190 °C for the different crystallization times (1–168 h).

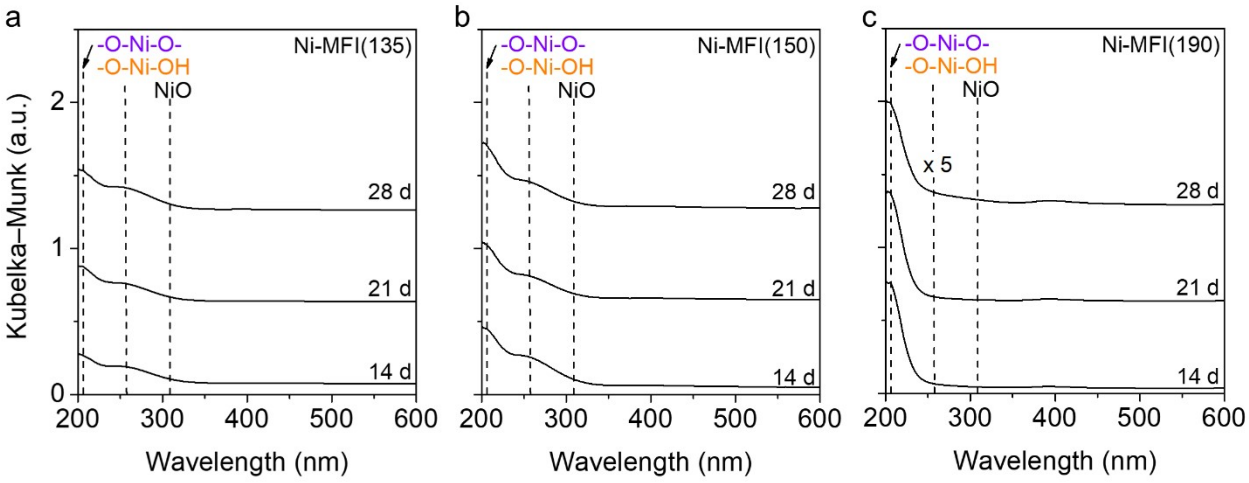

Fig. S16 UV-DRS spectra of Ni-MFI(x)(y) solids synthesized at (a) 135 °C, (b) 150 °C, and (c) 190 °C for 14–28 d.

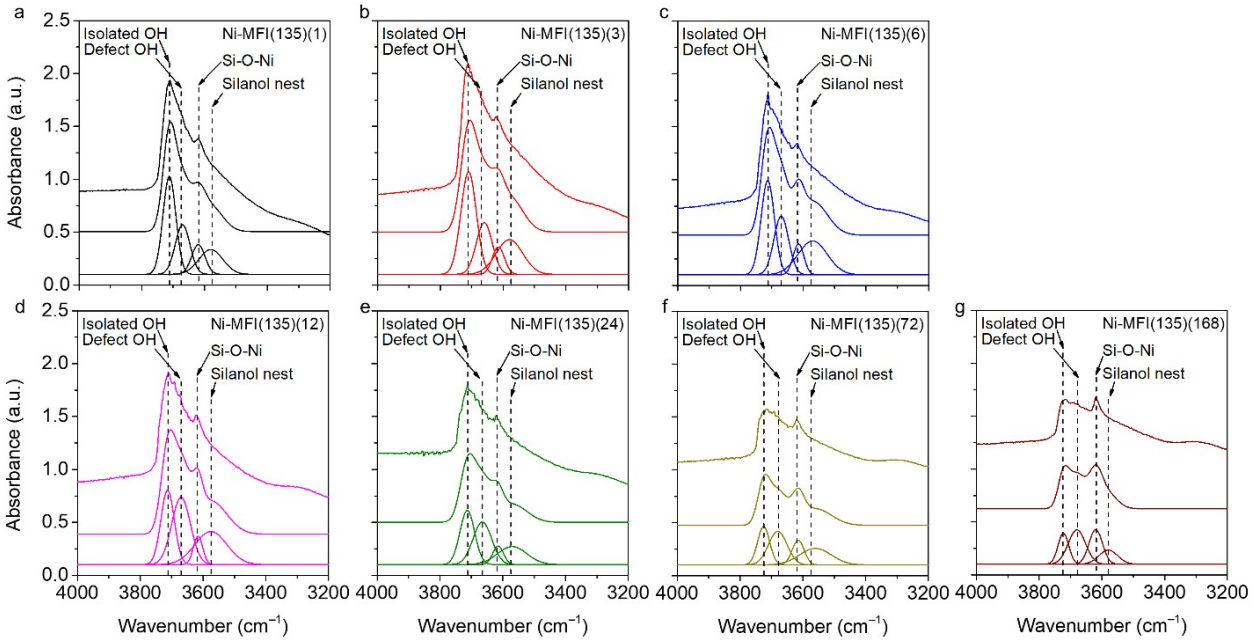

Fig. S17 IR spectra in the hydroxyl region of Ni-MFI(x)(y) solids synthesized at 135 °C for (a) 1 h, (b) 3 h, (c) 6 h, (d) 12 h, (e) 24 h, (f) 72 h, and (g) 168 h: experimental (top), simulated (middle), and deconvoluted components (bottom).

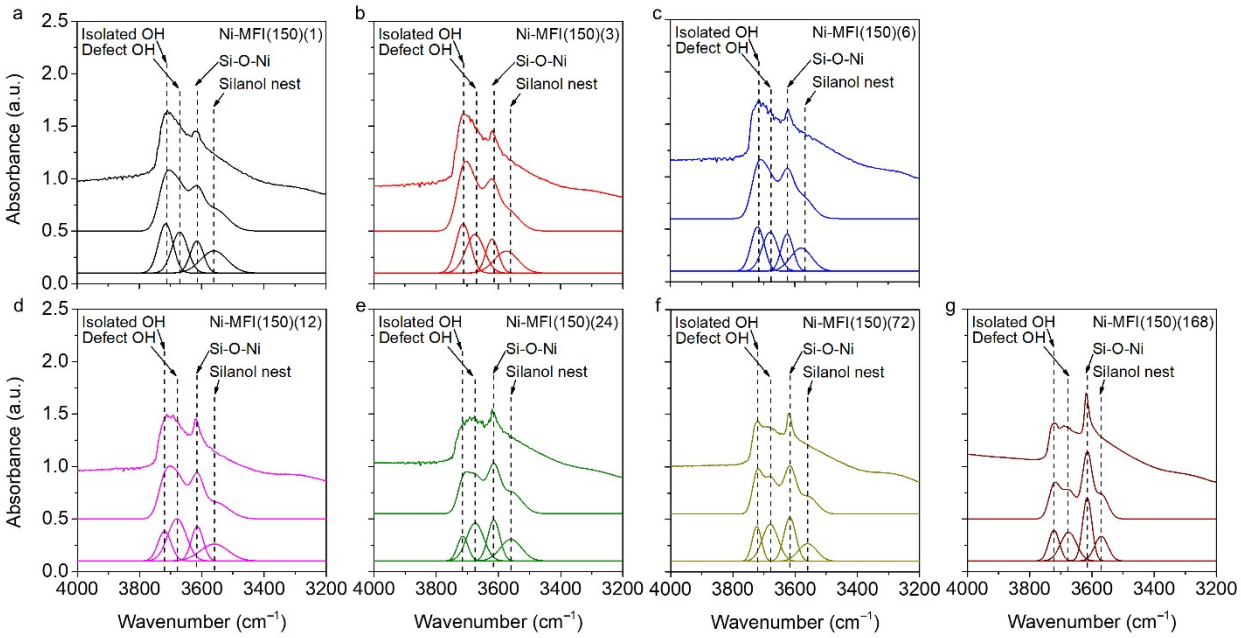

Fig. S18 IR spectra in the hydroxyl region of Ni-MFI(x)(y) solids synthesized at 150 °C for (a) 1 h, (b) 3 h, (c) 6 h, (d) 12 h, (e) 24 h, (f) 72 h, and (g) 168 h: experimental (top), simulated (middle), and deconvoluted components (bottom).

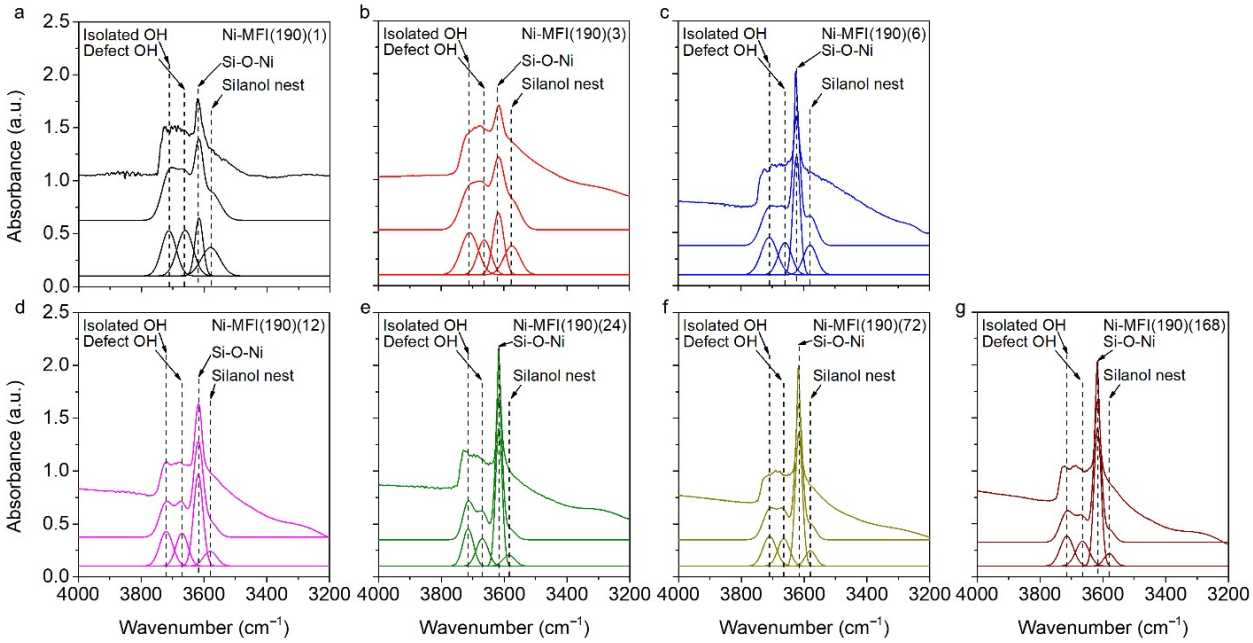

Fig. S19 IR spectra in the hydroxyl region of Ni-MFI(x)(y) solids synthesized at 190 °C for (a) 1 h, (b) 3 h, (c) 6 h, (d) 12 h, (e) 24 h, (f) 72 h, and (g) 168 h: experimental (top), simulated (middle), and deconvoluted components (bottom).

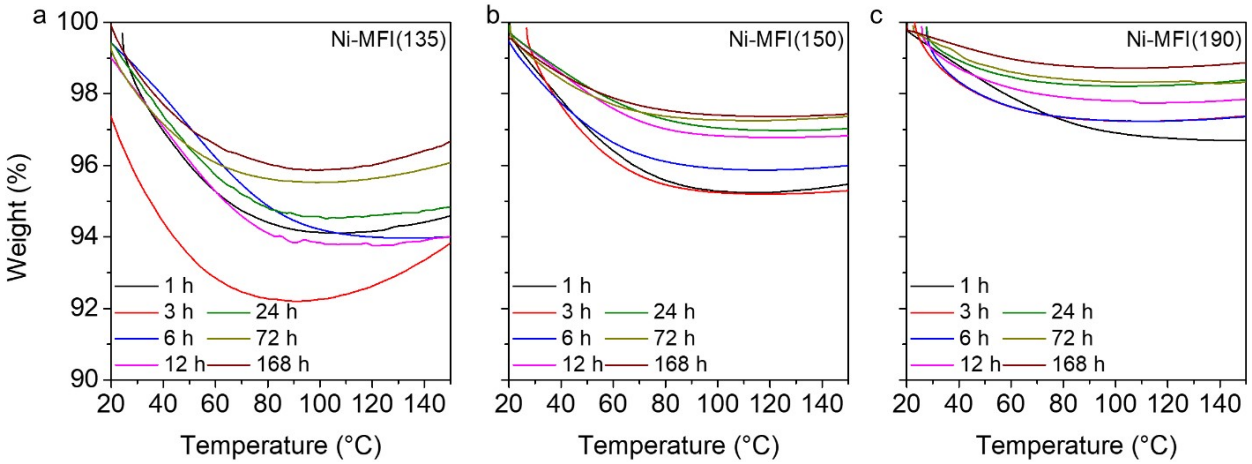

Fig. S20 TGA curves up to 150 °C of calcined Ni-MFI(x)(y) solids synthesized at (a) 135 °C, (b) 150 °C, and (c) 190 °C for the different crystallization times (1–168 h). Before the measurements, the calcined samples were exposed for 1 d in ambient condition.

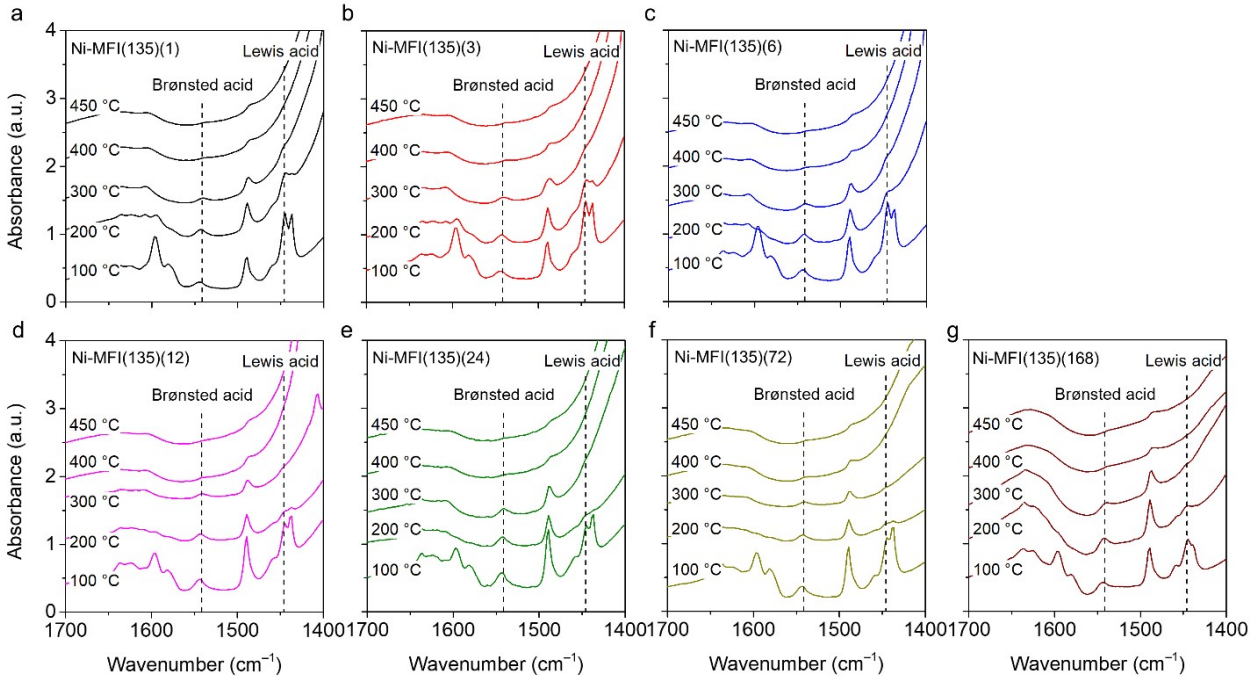

Fig. S21 IR spectra after pyridine adsorption at 100 °C and subsequent temperature increase up to 450 °C at an interval of 100 °C (100 to 400 °C) and 50 °C (400 to 450 °C) of Ni-MFI(*x*)(*y*) solids synthesized at 135 °C for (a) 1 h, (b) 3 h, (c) 6 h, (d) 12 h, (e) 24 h, (f) 72 h, and (g) 168 h.

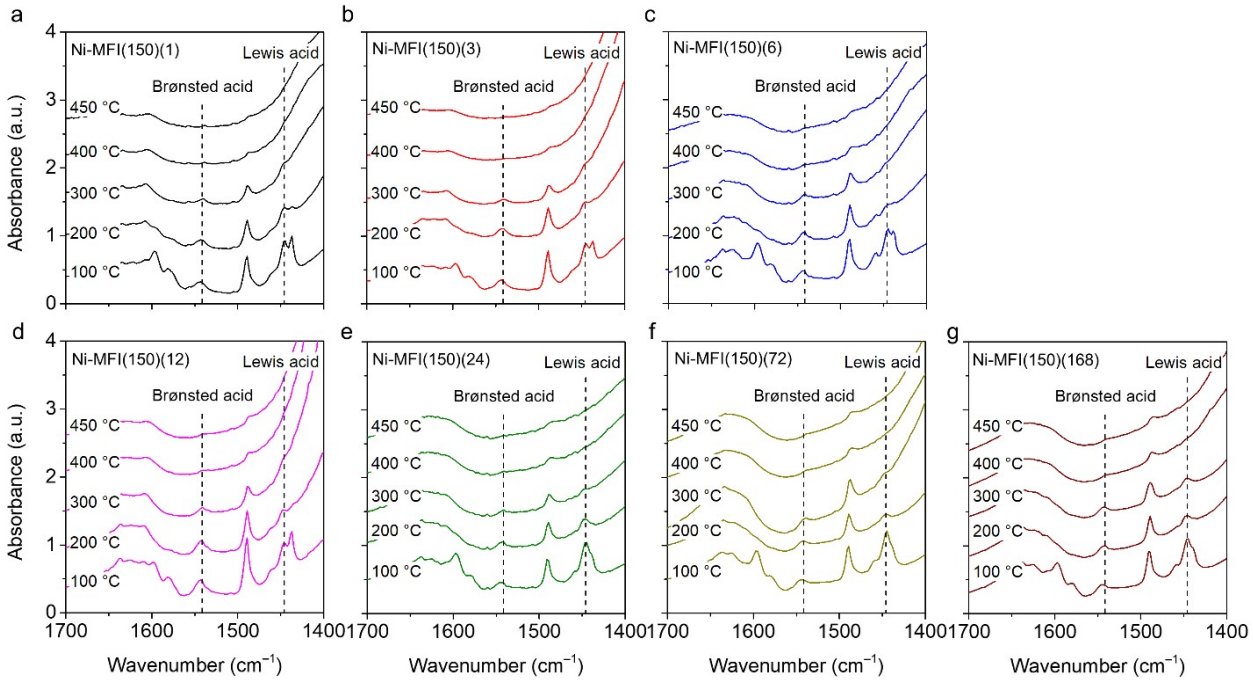

Fig. S22 IR spectra after pyridine adsorption at 100 °C and subsequent temperature increase up to 450 °C at an interval of 100 °C (100 to 400 °C) and 50 °C (400 to 450 °C) of Ni-MFI(x)(y) solids synthesized at 150 °C for (a) 1 h, (b) 3 h, (c) 6 h, (d) 12 h, (e) 24 h, (f) 72 h, and (g) 168 h.

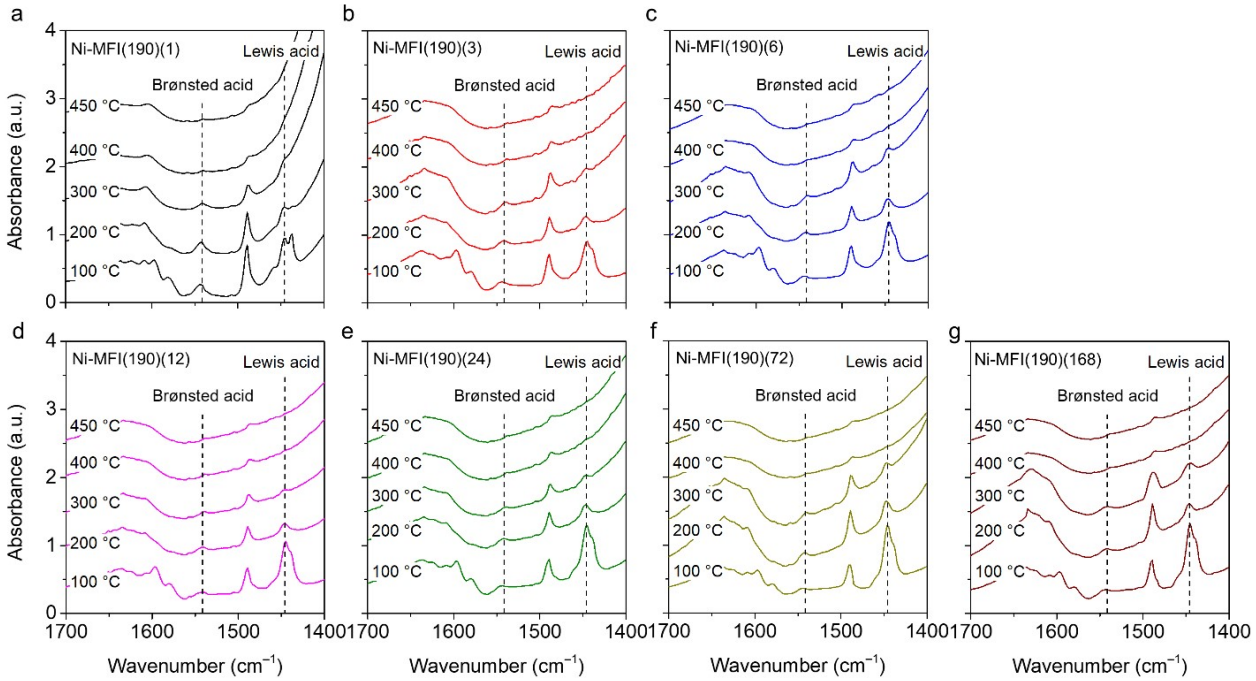

Fig. S23 IR spectra after pyridine adsorption at 100 °C and subsequent temperature increase up to 450 °C at an interval of 100 °C (100 to 400 °C) and 50 °C (400 to 450 °C) of Ni-MFI(*x*)(*y*) solids synthesized at 190 °C for (a) 1 h, (b) 3 h, (c) 6 h, (d) 12 h, (e) 24 h, (f) 72 h, and (g) 168 h.

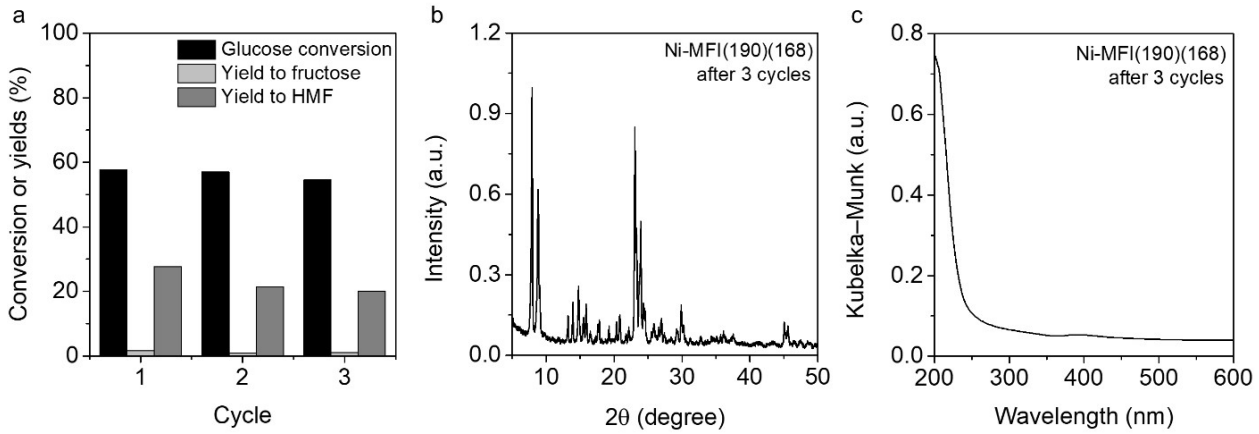

Fig. S24 (a) Reusability test results of Ni-MFI(190)(168) catalyst at 160 °C for 24 h in three consecutive runs. (b) Powder XRD pattern and (c) UV-DRS spectrum of Ni-MFI(190)(168) after the reusability test.